Petroleum and Coal

Article **Open Access**

Process Design and Operational Optimisation of a C3MR LNG Liquefaction Process Using Mathematical Modeling and Thermodynamic Analysis

Adel Omar, M. S. Awad, S. M. Aly

Petroleum Refining and Petrochemical Engineering Department, Faculty of Petroleum and Mining Engineering, Suez University, Suez, Egypt

Received July 30, 2023; Accepted November 13, 2023

Abstract

LNG liquefaction process is energy and cost intensive. Minimisation of energy consumption is the main target of LNG liquefaction process design and operational optimisation. A new mathematical programming methodology for optimisation of LNG liquefaction process is presented. The proposed methodology links mathematical programming and thermodynamic analysis to construct a MINLP (Mixed Integer Nonlinear Programming) model. Rigorous thermodynamic analysis was carried out to build Excel-based thermodynamic property models. Excel models were linked to GAMS through GDXXRW (GAMS Data Exchange) facility. Based on the developed model, LINDO global solver in GAMS was used to address the MINLP problem, and the optimisation results were eventually verified by detailed simulation. In parallel, optimal design and operational conditions can be achieved. To depict the efficacy of the new methodology, a C3MR LNG liquefaction process case study was investigated where the total energy consumption of the compressor was reduced by 15.77%. Deep thermodynamic analysis was performed to provide complete understanding of the process.

Keywords: *Mathematical programming; LNG liquefaction; Optimisation; C3MR liquefaction process; MINLP.*

1. Introduction

Recognized as the cleanest fossil fuel, natural gas has grown to be one of the mainstays of world energy where it improves air quality and limits carbon dioxide emissions. Directly, the global LNG demand has significantly escalated, driven by recent geopolitical changes and the incurred potential disruptions to natural gas supply to Europe. In natural gas liquefaction process, natural gas is refrigerated from ambient temperature to about -160°C. The United States Energy Information Administration (EIA) [1] pointed out that the volume of liquefied natural gas is approximately 600 times smaller than the volume of natural gas in its gaseous state. Hence natural gas may be shipped practically everywhere owing to the adaptability of LNG. The International Gas Union (IGU) world LNG report 2022 [2] stated that about 6.9 million tonnes per annum MTPA of liquefaction capacity were brought online in 2021, increasing global liquefaction capacity to 459,9 MTPA at the end of the year. Through2020 to 2021, international LNG trade increased by 4.5% reaching a record-setting level of 372.3 million tonnes MT.

Essentially, liquefaction of natural gas requires the removal of sensible and latent heat energy. The cascade cycle, the mixed refrigerant cycle, and the expander cycle are the three most common techniques for liquefying natural gas. The propane precooled mixed refrigerant process, known as C3MR, was developed by Air Products and Chemicals Inc. (APCI). It has gained a promising popularity in the liquefaction industry with one of the largest capacities that can reach up to 5 MTPA. Shell Inc. supposes that having a mixed refrigerant on the first cycle allows Shell's double mixed refrigerant dual mixed refrigerant process to get over some restrictions in C3MR process such as the propane compressor large size and the high Mach number at the end of the blades. In recent years, some novel three-cycle processes such as

the ConocoPhillips Optimised Cascade and the AP-X™ have become the proper choice for new LNG projects in Egypt and Qatar as mentioned by Primabudi *et al.* [3].

LNG liquefaction process is an energy-demanding process that involves considerable amounts of compression power. Therefore, minimizing the compressor power requirement shall be the main target of process design and operation in LNG industry. Process configuration, operational conditions, refrigerant flow rate, and mixed refrigerant composition should be prioritized during LNG process design and operational optimisation.

Vaidyaraman and Maranas [4] thoroughly explored the design of mixed refrigerant cascade processes. They incorporated a non-convex nonlinear program that describes the synthesis problem into an optimisation model. Jensen and Skogestad examined the most efficient performance of basic refrigeration cycles. In addition to the degrees of freedom [5], they considered the optimum level of sub-cooling, and the selection of controlled variables [6]. Yet, they did not focus on thermodynamic analysis in operational and control areas. Aspelund *et al.* [7] created a gradient-free optimisation-simulation technique for Aspen HYSYS-simulated processes. The Tabu-Search (TS) and Nelder-Mead-Downhill Simplex (NMDS) algorithms served as the basis for their optimisation procedure. Nondeterministic search methods were used to acquire optimal solutions by fine-tuning the TS-generated local optimal solutions with NMDS in order to decrease the number of simulations. Alabdulkarem *et al.* [8] optimised a propane pre-cooled mixed refrigerant LNG facility using a genetic algorithm from MATLAB's optimisation toolbox that was initially created by Mortazavi *et al.* [9]. The LNG plant's computer model was constructed with HYSYS and validated with an ASPEN Plus model built by Mortazavi *et al*. [9].

Shirazi and Mowla [10] utilised genetic algorithm as an optimisation method in which thermodynamic principles and parameters are calculated in MATLAB programme to produce the objective function. In order to optimise the variables of a single-staged mixed refrigerant SMR process, the Peng-Robinson equation of state was incorporated as an automatic procedure within the genetic algorithm method. Khan *et al.* [11] performed a study that harnessed the sequential coordinate randomization search method to optimise LNG (liquefied natural gas) process plants. Minimizing the multivariable function considering one variable at a time was the target on which the coordinate search was based. They incorporated randomness into the coordinated search in order to exhaustively explore the space of decision variables. Ghorbani *et al.* [12] used a combination of pinch and exergy analysis to attain the maximal exergetic efficiency. They also performed an exergoeconomic analysis using the total revenue requirement method. A coded genetic algorithm from Matlab software was linked to HYSYS software to determine the optimal performance of a propane-mixed refrigerant process. For two singular objective functions, optimisation of the previously mentioned system was conducted. One of the objective functions sought to minimise the unit cost of exergy, while the other aimed to maximise the system's exergetic efficiency. Elfakharany et al. performed minor structural modifications of the C3MR cycle to reduce the shaft power of the compressor by about 2.2 (MW/MTPA LNG) that resulted in an increased coefficient of performance (COP) of the refrigeration cycle [13].

Notable is the fact that nondeterministic search methods used in some optimisation studies are unable to predict a global optimal in an acceptable span of time. Wang *et al.* [14] performed a study that combined comprehensive thermodynamic analysis, detailed simulation, and optimisation in order to minimise the energy use of a propane precooled liquefaction process. Still, they did not establish a synthesis superstructure and the manipulated variables were omitted during the optimisation. Later, Wang *et al.* [15] proposed a novel MP method for LNG liquefaction synthesis with the goal of minimising energy consumption. Their method relied on mathematical programming, thermodynamic analysis, and thorough simulation. In their work, a process superstructure was constructed, and a MINLP model was developed, then simplified. The MINLP problem was resolved using the GAMS LINDO global solver. However, their work on thermodynamic analysis was primarily based on regression to simplify thermodynamic property functions, rather than actual and realistic thermodynamic calculations.

Edgar *et al.* [16] stated that deterministic optimisation methods and Mathematical Programming (MP) have proven to be more reliable in optimisation. They explained that these models are able to identify the optimal solution for the mathematical model representing the case and

its constraints. Using equation-based programmes and global solvers, according to Floudas [17], can ensure the global optimal solution availability. Mathematical Programming and deterministic search methods are seldom used in the optimisation of LNG refrigeration system, although they are preferable to heuristic and nondeterministic search methods [15]. This is attributed to the complexity of thermodynamic equations that makes it hard to incorporate thermodynamic functions into mathematical optimisation models.

In this paper, a new mathematical-programming-based method for LNG liquefaction process design and operational optimisation is constructed. A MINLP model is constructed to minimise total compressor shaft work based on the LNG liquefaction flow sheet superstructure described by Wang *et al.* [15]. Thermodynamic properties are first formulated with Peng-Robinson equation of state [18], then modeled in Excel spreadsheets before GDXXRW, GAMS Data Exchange (GDX) facility, is employed to link them with GAMS [19]. Then, the optimisation case is addressed through GAMS LINDO global solver. This model is partially inspired by the model and approach introduced by Wang *et al.* [15], where some important and clear modifications were applied in design equations. Optimisation results are further identified and tested by rigorous simulations. Both the design and operation of the LNG liquefaction process can be optimised simultaneously. The created model is demonstrated using the C3MR LNG liquefaction case, which is used in the research conducted by Wang *et al.* [15]. The process is thermodynamically analysed in depth to provide a full picture.

2. Methodology framework

Fig. 1 depicts the established methodology framework. It comprises three fundamental phases: Model structure construction, MINLP model formulation, and solution verification. In the initial phase, process analysis is used to determine the optimisation objectives. Afterwards, the proper structure for the LNG liquefaction process is constructed.

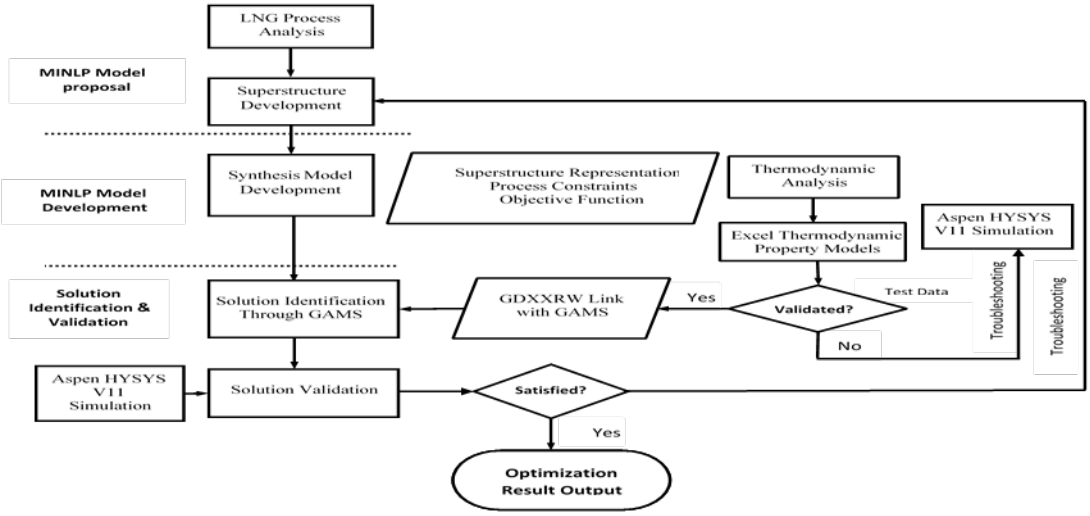

Fig. 1. Methodology framework.

The second phase involves the formulation of a MINLP model that is supported on the pertinent superstructure. In the formulation of the synthesis model, mass and energy balance equations, as well as thermodynamic functions, which are the building blocks of the optimisation model, demonstrate various unit operations. We managed to construct a general thermodynamic property model using Excel Spreadsheets despite the fact that the majority of thermodynamic functions are highly nonlinear and complex. PENG-ROB equation of state is embedded into Excel Spreadsheets to evaluate thermodynamic properties of streams based on detailed thermodynamic analysis of the process. This model is primarily verified to be accurate based on thorough simulation results using Aspen HYSYS V11. Aspen Tech Inc. [20] recom-

mend the application of Peng-Robinson equation of state as the thermodynamic property procedure for modelling given that it is an ideal choice for natural gas processing, petroleum refining, and petrochemical operations. After verifying Excel thermodynamic property models, GDXXRW, a GAMS Data Exchange (GDX) facility is used to link the Excel models with GAMS.

In the third phase, LINDO global solver is exploited for solving the optimisation problem with the built synthesis model. To further confirm the validity of identified solutions after obtaining optimisation results, the data output will again be input into Aspen HYSYS V11 to carry out the required simulation for validation of results. If the validation is unsuccessful, the preceding troubleshooting steps will be repeated until an accredited solution is obtained.

3. C3MR synthesis model

3.1. Process design

Fig. 2 represents the process flow diagram of the developed structure for the propane precooled mixed refrigerant C3MR process. Typical compositions of natural gas feed and mixed refrigerant streams employed in this study are the same compositions used in the study carried out by Wang *et al.* [15]. The mole fractions of the feed natural gas components are listed in Table 1. The temperature and pressure of the natural gas feed in the base case are 25°C and 52 bar respectively.

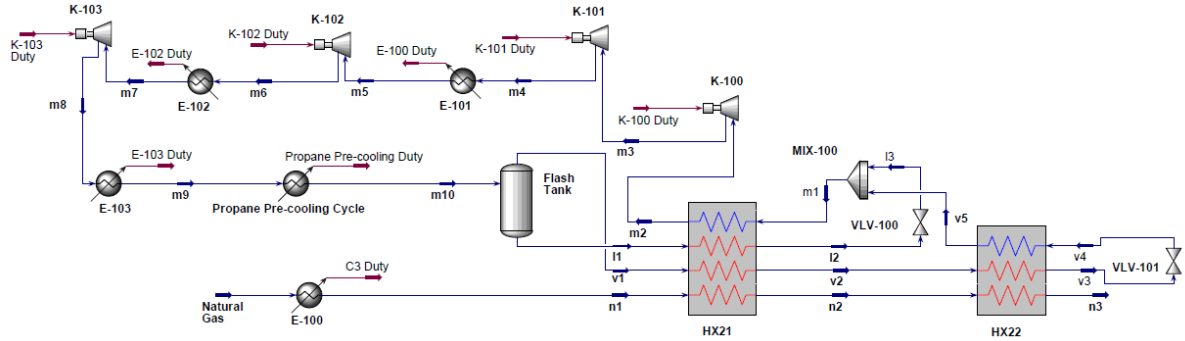

Fig. 2. Developed superstructure for propane pre-cooled mixed refrigerant C3MR process.

Table 1. Composition of natural gas feed stream.

Component	Mole fraction	Component	Mole fraction
Methane	0.95310	n- Butane	0.00060
Ethane	0.03350	Iso-Pentane	0.00002
Propane	0.00570	n-Pentane	0.00005
Iso-Butane	0.00090	Nitrogen	0.00600

The mole ratio composition of the mixed refrigerant stream is 8% nitrogen, 46% methane, and 46% ethane where the mass flow rate of the mixed refrigerant in the base case is 9020 kg/h. The entire C3MR procedure includes two chilling cycles: the propane precooling cycle and the main MR cycle. Using a series of propane heat exchangers, natural gas and mixed refrigerant streams are pre-cooled to approximately-40°C. This sequence is an element of the propane precooling cycle. After that, natural gas directly reaches the cold box; major cryogenic heat exchangers (MCHEs, HX21 and HX22), while the mixed refrigerant is directed to a flash drum where it is separated into a vapour stream (LMR: light mixed refrigerant) and a liquid stream (HMR: heavy mixed refrigerant). The LMR and HMR streams then take distinct paths during the mixed refrigerant cooling cycle. The liquid stream enters HX21 where it is subcooled and then throttled to normal pressure in a Joule–Thompson (JT) valve; meanwhile, its temperature is reduced to allow it to subsequently cool down all the hot inlet streams of HX21. In an identical manner, the vapour stream is liquefied and sub-cooled in HX21 and HX22 prior to

expansion through a Joule–Thompson (JT) valve. Afterwards, the vapour stream attains a sufficiently low temperature and cools down all the hot inlet streams of HX22. The vapour and liquid streams subsequently merge to form the cold stream in HX21. Before entering a four-stage compressor, the cold inlet stream of HX21 is vaporised and superheated. After compression and water chilling, the mixed refrigerant stream's refrigeration cycle is completed. Eventually, the natural gas is liquefied and chilled down to -160°C after emerging from the mixed refrigerant cooling series. Owing to the fact that the single-component refrigeration system is already highly developed, the potential for optimising the propane chilling cycle is somewhat constrained, Wang *et al.* [15]. This study does not consider the design and basic operating parameters of the propane precooling series during the synthesis and optimisation of the LNG liquefaction process.

In fact, the entire propane precooling series can be described as a virtual heat exchanger that chills the natural gas and the mixed refrigerant streams to-40°C. The calculation procedure of compression stages applied by Ludwig [21] is employed in this study. Accordingly, Four-stage compression is adopted, based on Ludwig's calculation procedure results. Inspired by Wang *et al.* [15], the designed structure addresses the possibilities for deciding on an inter-stage water-cooler within two subsequent compression stages, taking into concern operational safety (inlet temperature to the following stage must be less than 30°C) and compression ratios pertaining to power expenditure. In the constructed MINLP model, binary variables will indicate whether or not the mixed refrigerant stream will transit through a water-cooler before joining the ensuing compression stage.

3.2. Heat exchanger model

In realistic representations of heat exchangers, energy conservation should take precedence. Let the cold inlet and outlet streams of the heat exchanger X be c_j^{in} and c_j^{out}, and the hot inlet and outlet streams be h_i^{in} and h_i^{out}. Beneath is a representation of the model equations for the heat exchanger X:

$$\sum_i \left(\dot{m}_{h_i}.\Delta H_{h_i}^X\right) = -\sum_j \left(\dot{m}_{c_j}.\Delta H_{c_j}^X\right) \quad (1)$$

$$\dot{Q}_{Hot}^X = -\dot{Q}_{Cold}^X \quad (2)$$

$$\Delta H_{h_i}^X = H_{h_i^{out}}^X - H_{h_i^{in}}^X \quad (3)$$

$$\Delta H_{c_j}^X = H_{c_j^{out}}^X - H_{c_j^{in}}^X \quad (4)$$

$$P_{h_i^{out}} = P_{h_i^{in}} - 0.5 \quad (5)$$

$$P_{c_j^{out}} = P_{c_j^{in}} - 0.5 \quad (6)$$

$$\dot{H}_k = \dot{m}_k(H_k) \quad (7)$$

where $h_i^{in} \epsilon \{v_1, l_1, n_1, v_2, n_2\}$; $h_i^{out} \epsilon \{v_2, l_2, n_2, v_3, n_3\}$; $c_{j,X}^{in} \epsilon \{m_1, v_4\}$; $c_{j,X}^{out} \epsilon \{m_2, v_5\}$; and $k \epsilon \{v_1, \dots, v_5, l_1, l_2, n_1, n_2, n_3, m_1, \dots, m_{10}\}$. $\dot{m}_k$ is the mass flow rate of stream at status k in (kg/h). $\dot{m}_{h_i}.\Delta H_{h_i}^X$ and $\dot{m}_{c_j}.\Delta H_{c_j}^X$ are hot and cold stream enthalpy change rates during heat exchange process in (kJ/h) respectively.

For heat exchanger X, $\dot{Q}_{Hot}^X$ and $\dot{Q}_{Cold}^X$ are the total hot stream and total cold stream heat duties respectively (kJ/h). Note that a 0.5 bar pressure drop is presumed for every stream passing through the heat exchanger. The pressures of mixed refrigerant streams entering heat exchangers are determined by the discharge pressure of the final compression stage. The outlet temperatures of heat exchangers are the main manipulated variables, so they are supposed to be optimised through the process. However, stream n_3 has to be at -160°C to conform to the process specifications. Note, also that during the optimisation procedure, the MR composition is kept fixed.

In order to guarantee the reliability of heat transfer, the difference in temperature between the cold and hot streams of an exchanger must satisfy a minimal threshold. And for simplicity,

losses in heat energy are ignored. Countercurrent flow exchanger is selected in this LNG liquefaction process. Each multistream heat exchanger in the superstructure has a single cold stream and multiple hot streams. For any exchanger with a minimum approach temperature difference ΔT_{min}, all hot streams must have a higher exit temperature than the corresponding cold stream by ΔT_{min}. Simultaneously, cold streams must have a lower temperature at their exit than the hottest hot stream entering the system by ΔT_{min}. Hasan *et al.* [22] recommended that heat transfer involved in LNG process should have a minimum approach temperature of about 1-3°C. Based on this report, we use a minimal internal temperature approach (MITA) value of 2℃. The aforementioned temperature restraints are expressed as follows for a heat exchanger X:

$$T_{h_{i,X}}^{out} \geq T_{C_{j,X}}^{in} + \Delta T_{min} \quad (8)$$

$$T_{h_X}^{in} = max\, i \left\{T_{h_{i,X}}^{in}\right\} \quad (9)$$

$$T_{C_{j,X}}^{out} \leq T_{h_X}^{in} - \Delta T_{min} \quad (10)$$

where $X \epsilon \{HX21, HX22\}$, $h_{i,X}^{in} \epsilon \{v_1, l_1, n_1, v_2, n_2\}$, $h_{i,X}^{out} \epsilon \{v_2, l_2, n_2, v_3, n_3\}$, $c_j^{in} \epsilon \{m_1, v_4\}$, and $c_j^{out} \epsilon \{m_2, v_5\}$. $T_{h_X}^{in}$ is the highest inlet hot stream temperature in heat exchanger X.

For $HX21$, the temperatures of hot inlet streams (v_1, l_1, n_1) are equal. The precooling cycle for propane defines these temperatures. Therefore, Eq. (9) has the potential to be written for $HX21$ as follows:

$$T_{h_X}^{in} = T_{h_{i,X}}^{in} \quad (11)$$

where $h_{i,X}^{in} \epsilon \{v_1, l_1, n_1\}, h_{i,X}^{out} \epsilon \{l_2, v_2, n_2\}, c_{j,X}^{in} \epsilon \{m_1\}$, and $c_{j,X}^{out} \epsilon \{m_2\}$.

For $HX22$, two hot inlet streams (v_2, n_2) are considered. A binary variable x is used to decide $T_{h_X}^{in}$. The binary variable is assigned to 1 if $T_{h_{1,X}}^{in}$ is greater than $T_{h_{2,X}}^{in}$, otherwise the value is set to zero if $T_{h_{1,X}}^{in}$ is less than $T_{h_{2,X}}^{in}$. This implies the following expressions for the temperature constraints in $HX22$:

$$T_{h_X}^{in} = xT_{h_{1,X}}^{in} + (1-x)T_{h_{2,X}}^{in} \quad (12)$$

$$T_{h_{1,X}}^{in} - T_{h_{2,X}}^{in} \leq xT^{max} \quad (13)$$

$$T_{h_{1,X}}^{in} - T_{h_{2,X}}^{in} \geq (1-x)T^{max} \quad (14)$$

where $h_{1,X}^{in} \epsilon \{v_2\}, h_{2,X}^{in} \epsilon \{n_2\}, h_{i,X}^{out} \epsilon \{v_3, n_3\}$, $c_{j,X}^{in} \epsilon \{v_4\}$, $c_{j,X}^{out} \epsilon \{v_5\}$, and T^{max} is a present upper temperature limit.

3.3. Compressor model

To attain the desired pressure in the MR refrigeration cycle, a four-stage steady-state model of centrifugal compressors is used in this paper. On the basis of typical industrial experience, the adiabatic efficiency of the compressor is estimated at 75% and the mechanical efficiency is presumed to be 100%. The adiabatic and polytropic compressor efficiencies are computed as follows, where Eqs. (16) - (18) are adapted from Schultz [23]:

$$\text{Adiabatic Efficiency} = \frac{\text{Isentropic Power Required}}{\text{Actual Power Required}} \times 100\% \quad (15)$$

$$\text{Polytropic Efficiency} = \frac{\left[\left(\frac{P_{out}}{P_{in}}\right)^{\frac{n-1}{n}} - 1\right] \times \left[\left(\frac{n}{n-1}\right) \times \left(\frac{k-1}{k}\right)\right]}{\left[\left(\frac{P_{out}}{P_{in}}\right)^{\frac{k-1}{k}}\right]} \times \text{Adiabatic efficiency} \quad (16)$$

where n is the polytropic exponent, and k is the isentropic exponent;

$$n = \frac{\log\left(\frac{P_{out}}{P_{in}}\right)}{\log\left(\frac{\rho_{out,actual}}{\rho_{in}}\right)} \quad (17)$$

$$k = \frac{\log\left(\frac{P_{out}}{P_{in}}\right)}{\log\left(\frac{\rho_{out,ideal}}{\rho_{in}}\right)} \quad (18)$$

Interstage water coolers are employed if the outlet temperature of the preceding compression stage exceeds 30℃ for safety considerations. The temperature at the output of each compression stage $T_{cp_n}^{out}$ becomes a decision parameter to determine the operational conditions of the compressor. Therefore, after each compression stage, there are two available paths for the outlet MR stream from each compression stage; either it undergoes cooling in water cooler to reach 30℃ or it directly flows to the following compression stage. This option has been modeled using a set of binary variables y_n. For the nth compression stage, the corresponding binary variable is assigned a value of 1 if the stage outlet temperature $T_{cp_n}^{out}$ is above 30°C the MR stream shall undergo cooling before entering the next stage of compression at an inlet temperature $T_{cp_{n+1}}^{in}$of 30°C. On the other hand, the binary variable will be of value zero if the temperature of the outlet stream from the compression stage is lower than 30 ℃, indicating that no cooling is applied after the corresponding state. Then, in this case, $T_{cp_n}^{out}$and $H_{C_{pn}^{out}}$ will represent the inlet temperature and enthalpy rate of the subsequent stage. The inlet temperature $T_{cp_1}^{in}$ and stream enthalpy $H_{cp_1}^{in}$ of the first compressor stage are determined by the temperature T_{m_2} and enthalpy $H_{m_2}$of the cold outlet stream m_2, respectively. The inter-stage pressures are decided by trial balancing; assuming that one half of the intercooler pressure drop, which is estimated to be 0.5 bar, is carried by each cylinder. The compressor model is formulated below:

$$T_{cp_1}^{in} = T_{m_2} \quad (19)$$

$$\dot{H}_{cp_1}^{in} = H_{m_2}.\dot{m}_{m2} \quad (20)$$

$$P_{cp_1}^{in} = 1\ bar = P_{m_2} \quad (21)$$

$$Cr_{uncorrected} = \sqrt[4]{P_{cp_4}^{out} / P_{cp_1}^{in}} \quad (22)$$

$$Cr_1 = Cr_{uncorrected} \quad (23)$$

$$Cr_n = P_{cp_n}^{out} / P_{cp_n}^{in}\ ; 2 \le n \le 4 \quad 24)$$

$$P_{cp_n}^{out} = (1 - y_n)Cr_{uncorrected}P_{cp_n}^{in} + y_n\left(Cr_{uncorrected}P_{cp_n}^{in} + 0.25\right); 1 \le n \le 3 \quad (25)$$

$$P_{cp_{n+1}}^{in} = (1 - y_n)P_{cp_n}^{out} + y_n\left(P_{cp_n}^{out} - 0.5\right); 1 \le n \le 3 \quad (26)$$

$$P_{cp_4}^{out} \le 55\ bar \quad (27)$$

$$1.5 \le Cr_n \le 3.5 \quad (28)$$

$$T_{cp_n}^{out} = T_{cp_n}^{in}(Cr_n)^{(k-1)/k}, T(K) \quad (29)$$

$$k = C_p / C_v \quad (30)$$

$$T_{cp_n}^{out} - 30 \le y_n T^{cmax} \quad (31)$$

$$T_{cp_n}^{out} - 30 \ge (y_n - 1)T^{cmax} \quad (32)$$

$$T_{cp_{n+1}}^{in} = 30y_n + T_{cp_n}^{out}(1 - y_n)\ ; 1 \le n \le 3 \quad (33)$$

$$\dot{H}_{cp_{n+1}}^{in} = \dot{m}_k(H_{cp_{n+1}}^{in})\ ; 1 \le n \le 3 \quad (34)$$

$$\dot{H}_{cp_n}^{out} = \dot{m}_k(H_{cp_n}^{out}) \quad (35)$$

where k is the ratio of specific heats, T^{cmax} represents the maximum compressor discharge temperature; set to be $150℃$. $Cr_{uncorrected}$ is the uncorrected compression ratio, and Cr_n is the compression ratio of nth stage.

$$\dot{W}_{cp_n} = \dot{H}_{cp_n}^{out} - \dot{H}_{cp_n}^{in} \quad (36)$$

$$\dot{W}_{total} = \sum_{n=1}^{4} \dot{W}_{cp_n} \quad (37)$$

The nth stage compressor shaft work $\dot{W}_{cp_n}$ equals the difference between the enthalpies of the outlet and inlet streams. Calculation of stream enthalpy rate is discussed in thermodynamics section afterwards.

3.4. Flash drum model

The mixed refrigerant stream undergoes cooling to $-40℃$ in the propane precooling cycle after the four-stage compression. A flash drum separates the two-phase stream m_{10} into the vapour stream v_1 and the liquid stream l_1. The following formulations represent the basis of the flash drum model calculations:

$$P_{m_{10}} = P_{cp_4}^{out} \quad (38)$$

$$T_{m_{10}} = -40℃ \quad (39)$$

$$\dot{m}_{m_{10}} = \dot{m}_{v_1} + \dot{m}_{l_1} \quad (40)$$

$$z_i\dot{n}_{m_{10}} = y_i\dot{n}_{v_1} + x_i\dot{n}_{l_1} \quad (41)$$

where $\dot{n}_k$ represents the stream molar flow rate at status k in $(kmol/h)$.

The MR stream reaches a high pressure of about 55 bar, so the drop in pressure in the flash drum may be ignored. Furthermore, since the loss of heat is minimal and can be neglected, the pressure and temperature of the discharge streams v_1 and l_1 are supposed to be the same as the inlet stream m_{10}. Properties of the inlet stream m_{10} can be computed from the compressor model equations. The compositions of the vapour x_i and liquid y_i streams are evaluated using Rachford-Rice procedure for flash distillation as will be explained in thermodynamic properties section. Based on mass balance equations, mass flow rate $\dot{m}_{l_1}$ and composition x_i of stream l_1 can be evaluated.

3.5. Process specifications

The produced LNG stream has to be settled at $-160℃$ after the natural gas feed stream is cooled down, liquefied, then eventually undergoes subcooling in the liquefaction process.

$$T_{n_3} = -160℃ \quad (42)$$

3.6. Objective function

Minimizing the total compression energy consumption is the main objective function of the LNG synthesis procedure. This is mathematically illustrated below:

$$min \quad \dot{W}_{total} = \sum_{n=1}^{4} \dot{W}_{cp_n} \quad (43)$$

To sum up, Eqs. (1) - (43) form the structure of the model equations. Four compression stages are utilised throughout the entire course of the optimisation procedure. Consequently, the major capital cost remains constant, so the primary concern is the cost of operation, which is primarily dependent on net compressor energy consumption. Heat exchanger outlet temperatures $T_{h_{i,X}}^{out}$ and $T_{C_{j,X}}^{out}$ represent manipulated variables. On the whole, these independent variables and the previously listed equations form a MINLP model.

4. Thermodynamic properties

Determining thermodynamic properties is a difficult endeavor. Engineers do practically exploit thermodynamic properties, and a comprehension of how they are calculated should suggest that every property value is subject to some degree of uncertainty. Thus, according to Smith *et al.* [24], precise data must be provided to obtain enthalpy and entropy estimations that are appropriate for engineering computations. In this work, Peng-Robinson equation of state Eqs. (44) - (57) serves as the basis for calculating thermodynamic properties and studying phase equilibrium.

4.1. Enthalpy calculations

Based on a rigorous thermodynamic study, methods for calculation of enthalpy of mixture fluid streams have been investigated. These methods vary according to the phase of material fluid stream where streams present in the relevant LNG process superstructure are vapour-phase, liquid-phase, or two-phase streams. PR equation of state is formulated as follows:

$$P = \frac{RT}{\underline{v} - b_m} - \frac{a(T)_m}{\underline{v}(\underline{v} + b_m) + b_m(\underline{v} - b_m)} \tag{44}$$

where

$$a(T)_m = \sum_i \sum_j \left[x_i\, x_j \left(a_i(T) a_j(T) \right)^{0.5} \left(1 - k_{ij}\right) \right] \tag{45}$$

$$a_{ij} = \left(a_i(T) a_j(T) \right)^{0.5} \left(1 - k_{ij}\right) \tag{46}$$

$$a_i(T) = a_i(T_{ci}).\, \alpha_i \tag{47}$$

$$a_i(T_{ci}) = \Omega_a \frac{R^2 T_{ci}^2}{P_{ci}} \tag{48}$$

$$\Omega_a = 0.45724 \tag{49}$$

$$\alpha_i = \left[1 + m_i \left(1 - {T_{ri}}^{0.5} \right) \right]^2 \tag{50}$$

$$m_i = 0.3746 + 1.5423\omega_i - 0.2699\omega_i^2 \tag{51}$$

$$b_m = \sum_i x_i b_i \tag{52}$$

$$\Omega_b = 0.07780 \tag{53}$$

$$b_i = \Omega_b \frac{RT_{ci}}{P_{ci}} \tag{54}$$

$$A_m = \frac{a(T)_m P}{R^2 T^2} \tag{55}$$

$$B_m = \frac{b_m P}{RT} \tag{56}$$

$$Z^3 + (B_m - 1)Z^2 + (A_m - 3B_m^2 - 2B_m)Z - (A_m B_m - B_m^2 - B_m^3) = 0 \tag{57}$$

4.1.1. Vapor mixtures

At temperature T, pressure P, and composition y_i, the calculation procedure of enthalpy of a real vapour-phase mixture fluid stream $H^V\,(T,\, P, y_i)$ is based on the following, where Eqs. (58) - (64) are adapted from Gmehling *et al.* [25]:

$$H^V\,(T,\, P, y_i) = H_{mix}^{id}(T,\, P, y_i) + H_{mix}^{R}(T,\, P, y_i) \tag{58}$$

$$H_{mix}^{R}(T,\, P, y_i) = (H^V - H^{id})_{mix}(T,\, P, y_i) \tag{59}$$

$$H^V\,(T,\, P, y_i) = H_{mix}^{id}(T,\, P, y_i) + (H^V - H^{id})_{mix}(T,\, P, y_i) \tag{60}$$

$$H_{mix}^{id}(T,\ P, y_i) = \sum_i y_i * H_{i\,(T,P)}^{id} \tag{61}$$

$$H_{i\,(T,P)}^{id} = \int_{T_0}^{T} C_{p_i}^{id} dT + \Delta h_{f_i}^0 \tag{62}$$

$$(H^V - H^{id})_{mix} = RT(Z^V - 1) + \frac{T\left(\frac{da}{dT}\right) - a}{2\sqrt{2}\,B_m} \ln\left[\frac{Z^V + (1+\sqrt{2})B_m}{Z^V + (1-\sqrt{2})B_m}\right] \tag{63}$$

$$\left(\frac{da}{dT}\right) = \frac{-\,m\,a}{\sqrt{\alpha T T_{pc}}} \tag{64}$$

$$m = \sum_i y_i m_i \tag{65}$$

$$\alpha = \sum_i y_i \alpha_i \tag{66}$$

$$C_{p_i}^{id}/_R = a_0 + a_1 T + a_2 T^2 + a_3 T^3 + a_4 T^4 \tag{67}$$

Such that $H_{mix}^{id}(T,\ P, y_i)$ and $H_{mix}^{R}(T,\ P, y_i)$ are the ideal-gas enthalpy $(kJ/kmol)$ and the residual enthalpy $(kJ/kmol)$ of a vapour mixture at pressure P, temperature T, and composition y_i respectively. $H_{i\,(T,P)}^{id}$ is the ideal-gas enthalpy of component i $(kJ/kmol)$. $C_{p_i}^{id}$ is the constant-pressure ideal-gas specific heat capacity $\left({}^{kJ}/_{kmol.K}\right)$. Eq. (67) is used by Poling *et al.* [26] to calculate $C_{p_i}^{id}$ where a_0, a_1, a_2, a_3, and a_4 are constants. For every component i, $\Delta h_{f_i}^0$ represents the standard heat of formation $(kJ/kmol)$. Z^V is the vapour-phase compressibility factor. T_{pc} gives the pseudocritical temperature of the mixture (K). R is the universal gas constant $\left({}^{kJ}/_{kmol.K}\right)$.

4.1.2. Liquid mixtures

At temperature T, pressure P, and composition x_i, the calculation procedure of enthalpy of a real liquid-phase mixture fluid stream $H^L(T,\ x_i)$ is based on the following, where Eqs. (68) - (75) are adapted from Gmehling *et al.* [25]:

$$H^L(T,\ x_i) = \sum_i x_i * H_i^L(T) \tag{67}$$

$$H_i^L(T) = \int_{T_0}^{T} C_{p_i}^{id} dT + \Delta h_{f_i}^0 + H_i^R\ (T,\ P_i^s) + \Delta h_{v_i} \tag{68}$$

$$H_i^R\ (T,\ P_i^s) = \left(H^L - H^{id}\right)_i\ (T,\ P_i^s) \tag{69}$$

$$H_i^L(T) = \int_{T_0}^{T} C_{p_i}^{id} dT + \Delta h_{f_i}^0 + \left(H^L - H^{id}\right)_i\ (T,\ P_i^s) + \Delta h_{v_i} \tag{70}$$

Gmehling *et al.* [25] noted that with this route, any liquid of a pure component is considered to be in the saturation state at the given temperature.

$$\ln P_i^s/_{P_{ci}} = \frac{1}{T_r}[A(1-T_{ri}) + B(1-T_{ri})^{1.5} + C(1-T_{ri})^{2.5} + D(1-T_{ri})^5] \tag{71}$$

$$\Delta h_{v_i} = RT_{ci}\left(A{\tau_i}^{1/3} + B{\tau_i}^{2/3} + C\tau_i + D{\tau_i}^2 + E{\tau_i}^6\right) \tag{72}$$

$$\tau_i = 1 - T/T_{ci} \tag{73}$$

$$(H - H^{id})_i\ (T,\ P_i^s) = RT(Z_i^s - 1) + \frac{T\left(\frac{da}{dT}\right)_i - a}{2\sqrt{2}\,B_i} \ln\left[\frac{Z_i^s + (1+\sqrt{2})B_i}{Z_i^s + (1-\sqrt{2})B_i}\right] \tag{74}$$

where P_i^s indicates component i saturation pressure (bar) at system temperature T. $H_i^L(T)$ represents the real liquid-phase enthalpy of component i in stream $(kJ/kmol)$. $H_i^R\ (T,\ P_i^s)$ denotes component i residual enthalpy $(kJ/kmol)$ at system temperature T, saturation pressure P_i^s. The

terms $\int_{T_0}^{T} C_{p_i}^{id} dT + \Delta h_{f_i}^0$ represent the ideal-gas enthalpy of component i $(kJ/kmol)$ at system temperature T. $C_{p_i}^{id}$ is the constant-pressure ideal-gas specific heat capacity $\left({}^{kJ}/_{kmol.K}\right)$. For every component i, $\Delta h_{f_i}^0$ and Δh_{v_i} are the standard heat of formation $(kJ/kmol)$, and the heat of vaporization $(kJ/kmol)$ at system temperature T respectively. Z_i^s represents the vapour-phase compressibility factor for component i at P_i^s. T_{ci} is the pseudocritical temperature of component i (K). R signifies the universal gas constant $\left({}^{kJ}/_{kmol.K}\right)$. Eqs. (72)-(73) are adapted from Gmehling *et al.* [25], where the relevant constants used in the equations are tabulated for each component i.

4.1.3. Liquid mixtures containing noncondensable components

In certain cases, we have a condensed phase with one or more components that cannot exist in the same condensed phase when pure and at the same temperature. Typically, this indicates that the temperature of the system exceeds the critical temperature of components, Tester and Modell [27]. This special case has been encountered in some liquid streams and in the liquid fraction of some two-phase streams inside the concerned LNG process model, where the mixed refrigerant or the natural gas mixture fluid stream exists, in liquid phase, above the critical temperature of one of the components, usually nitrogen. Within this case, nitrogen shall then be treated as a hypothetical liquid or a supercritical gas; a noncondensable component (at infinite dilution). There is no liquid phase and, consequently, no values for v_i and Δh_{v_i} for supercritical gases, Gmehling et al. [25].

Eq. (76) was suggested by Prausnitz *et al.* [28] to calculate the enthalpy of liquid mixtures containing noncondensable components. The Equation is formulated as follows:

$$H^L(T, x_i) = H^{id}(T, x_i) - \underbrace{\sum_{i=1}^{m} x_i RT^2 \left({}^{\partial \ln \gamma_i^{(P0)}}/_{\partial T}\right)_{P,x} - \sum_{i=1}^{m} x_i RT^2 \left({}^{d \ln f_i^{(P0)}}/_{dT}\right)_{Pure}}_{all\ condensables} \underbrace{- \sum_{i=1}^{m} x_i RT^2 \left({}^{\partial \ln \gamma_i^{\infty}}/_{\partial T}\right)_{x} - \sum_{i=1}^{m} x_i RT^2 \left({}^{d \ln f_i^{0L}}/_{dT}\right)}_{all\ noncondensables} \quad (75)$$

where the first term gives the ideal-gas enthalpy of mixture, the second and third terms give the excess enthalpy and the ideal liquid enthalpy, corrected to zero pressure, for all condensables respectively. And the fourth and fifth terms give the excess enthalpy and the ideal liquid enthalpy, corrected to zero pressure, for all noncondensables respectively.

The term that accounts for excess enthalpy of noncondensables $\left(-\sum_{i=1}^{m} x_i RT^2 \left({}^{\partial \ln \gamma_i^{\infty}}/_{\partial T}\right)_x\right)$ is ignored; its contribution to the total liquid enthalpy is not large as mentioned by Prausnitz. Therefore, a part of this equation is used to determine the enthalpy of noncondensable components at infinite dilution in a mixture. For noncondensables:

$$H^L(T, x_i) = H^{id}(T, x_i) - \sum_{i=1}^{m} x_i RT^2 \left({}^{d \ln f_i^{0L}}/_{dT}\right) \quad (76)$$

In this paper, the enthalpy of non-condensable nitrogen in liquid mixtures is calculated as follows:

$$H^{id}(T, x_i) = x_{N_2} H_{N_2}^{id} \quad (77)$$

$$H_{N_2}^{id} = \int_{T_0}^{T} C_{p_{N_2}} dT + \Delta h_{f_{N_2}}^0 \quad (78)$$

$$\left({}^{d \ln f_i^{0L}}/_{dT}\right) = 7.534\, T_{c_{N_2}}^{-1} T^{-2} - 2.598\, T^{-1} \quad (79)$$

$$H_{N_2}^{L}\left(T, x_{N_2}\right) = x_{N_2} H_{N_2}^{id} + x_{N_2} R \left(7.534\, T_{c_{N_2}}^{-1} - 2.598\, T\right) \quad (80)$$

where f_i^{0L} is the standard-state fugacity of pure liquid i at system temperature, given by

$$\ln {f_i^{0L}}/{P_{ci}} = 7.224 - 7.534\left(\frac{T}{T_{ci}}\right)^{-1} - 2.598\ln\left(\frac{T}{T_{ci}}\right) \quad (81)$$

T_{ci} and P_{ci} designate the critical temperature (K) and pressure (bar) of component i respectively.

4.1.4. Two-phase vapor-liquid systems

Enthalpy of a two-phase system is equal to the sum of the enthalpies of the vapour and liquid phases. The relation is generalized as follows:

$$H = x^L H^L + x^V H^V \quad (82)$$

where x^V denotes the mole fraction of the vapour portion of the system; quality of the system. x^L represents the mole fraction of the liquid portion of the system.

4.2. Phase equilibrium calculations

Phase equilibrium calculations for the flash drum model are thoroughly conducted using Rachford-Rice procedure [29] for isothermal flash distillation. These calculations are carried out to get the composition and mass flow rate of vapour and liquid phase streams produced from the flash drum. An iterative solution, using Newton's Method [30] is applied to get vapour to liquid molar flow ratios $({n_V}/{n_L})$ at equilibrium, and hence, vapour and liquid phase compositions are obtained easily. Setting a basis of one mole of the two-phase mixture, the calculation procedure is expressed below:

$$n_t = 1 = n_V + n_L \quad (83)$$

$$z_i = y_i n_V + x_i n_L \quad (84)$$

$$y_i = x_i K_i \quad (85)$$

$$x_i = \frac{z_i}{n_L + K_i n_V} \quad (86)$$

$$y_i = \frac{z_i K_i}{n_L + K_i n_V} \quad (87)$$

$$\sum_i x_i = 1 \quad (88)$$

$$\sum_i y_i = 1 \quad (89)$$

$$\sum_i y_i - \sum_i x_i = 0 \quad (90)$$

Then,

$$f(n_V) = \sum_i \frac{z_i(K_i - 1)}{n_V(K_i - 1) + 1} = 0 \quad (91)$$

Iterations are carried out by applying the basic expression for Newton's Method:

$$(n_V)_n = (n_V)_{n-1} - \frac{f((n_V)_{n-1})}{f'((n_V)_{n-1})} \quad (92)$$

where

$$f'((n_V)_{n-1}) = \sum_i \frac{z_i(K_i - 1)^2}{(n_V(K_i - 1) + 1)^2} \quad (93)$$

where n_V and n_L are mole fractions of vapour and liquid respectively. K_i signifies the vapour-liquid equilibrium ratio (K-factor) of component i. y_i and x_i are the vapour and liquid stream compositions respectively. z_i is the mole fraction of feed stream to the flash drum.

Upon reaching an acceptable relative tolerance of numerical value 1.0×10^{-5}, the value of n_V becomes acceptable. Henceforth, vapour to liquid molar flow ratios $({n_V}/{n_L})$, and resulting vapour and liquid stream compositions x_i and y_i become available using Eqs (87) and (88).

In this work, the calculation of vapour-liquid equilibrium ratios (K-factors) is predicated on Peng-Robinson equation of state approach, where liquid-phase fugacity is calculated using the following formula:

$$\ln \varphi_i^L = \frac{b_i}{b_m}(Z^L - 1) - ln(Z^L - B_m) + \frac{A_m}{2\sqrt{2}B_m}\left(\frac{2\psi_i}{a(T)_m}\frac{b_i}{b_m}\right)\ln\left[\frac{Z^L + (1+\sqrt{2})B_m}{Z^L + (1-\sqrt{2})B_m}\right] \quad (94)$$

where

$$\psi_i = \sum_j x_j a_{ij} \quad (95)$$

$$a(T)_m = \sum_i x_i * \psi_i \quad (96)$$

φ_i^L indicates component i liquid-phase fugacity coefficient, and ψ_i marks a parameter depending in the PR cross-attraction parameter a_{ij} for components i and j.

In the above equations, some mathematical expressions are written for the liquid phase, and the corresponding expressions are similarly obtained for the vapour phase doing Z^V instead of Z^L and y_i instead of x_i, wherever appropriate. Therefore, the values of equilibrium ratios are obtained from the quotient of liquid-phase and vapour-phase fugacity coefficients.

$$K_i = \frac{y_i}{x_i} = \frac{\varphi_i^L}{\varphi_i^V} \quad (97)$$

5. Results and discussion

Thermodynamic properties are thoroughly formulated and calculated using detailed Excel spreadsheets. GDXXRW, one of the most promising GAMS Data Exchange (GDX) utilities, that is used to read and write Excel spreadsheet data, is used to link the thermodynamic data of streams in Excel with GAMS. Being formulated with GAMS, the constructed model for LNG synthesis has been solved by LINDO global solver. The LINDO global optimisation method (GOP) uses branch-and-cut techniques to decompose an NLP model into a series of subproblems. Every subproblem is examined, and either indicated not to have a feasible or optimal solution, or an optimum solution is identified because the subproblem seems convex, or the subproblem is further broken down into two or more problems, which are then added to the list, LINDO API 13.0 [31]. 1338.88 kW is the global optimal solution for the MINLP problem. For further validation of optimisation results obtained from Excel-based thermodynamic property calculations and GAMS, rigorous simulations have been carried out. Table 2 and 3 depict the comparison between values of calculated thermodynamic properties and those obtained by HYSYS simulations. In general, the results are quite matching well where the majority of relative errors are under 1% and the greatest relative error is 3.5%. Therefore, the proposed thermodynamic models for computing thermodynamic properties have proved to be of high accuracy. Table 4 shows how optimisation results have fulfilled the goal of minimising energy consumption. The net compressors shaft work declined from $1589.56\ kW$ to $1338.88\ kW$ resulting in energy savings of 15.77%. Table 4 and 5 summarise the operational status for base and optimised cases.

Table 1. Enthalpy rate comparison between thermodynamic analysis and HYSYS simulation.

Variables	Thermodynamic analysis (GJ/h)	Simulation (GJ/h)	Relative Error (%)
H_{v1}	-7.95	-7.90	0.66
H_{v2}	-9.11	-9.00	1.23
H_{v3}	-9.16	-9.06	1.09
H_{v4}	-9.03	-9.06	0.38
H_{v5}	-8.54	-8.57	0.44
H_{l1}	-24.48	-24.04	1.81

Variables	Thermodynamic analysis (GJ/h)	Simulation (GJ/h)	Relative Error (%)
H_{l2}	-25.72	-25.27	1.74
H_{l3}	-25.21	-25.27	0.24
H_{m1}	-33.83	-33.85	0.05
H_{m2}	-29.33	-29.36	0.08
H_{n1}	-18.86	-18.83	0.15
H_{n2}	-20.96	-20.98	0.10
H_{n3}	-21.42	-21.40	0.09
$H_{cp_1^{in}} = H_{m2}$	-29.33	-29.36	0.08
$H_{cp_2^{in}} = H_{m3}$	-28.53	-28.29	0.86
$H_{cp_3^{in}} = H_{m5}$	-28.29	-28.25	0.16
$H_{cp_4^{in}} = H_{m7}$	-28.45	-28.40	0.16
$H_{cp_1^{out}} = H_{m3}$	-28.53	-28.29	0.86
$H_{cp_2^{out}} = H_{m4}$	-27.23	-26.85	1.40
$H_{cp_3^{out}} = H_{m6}$	-26.90	-26.85	0.18
$H_{cp_{14}^{in}} = H_{m8}$	-27.13	-27.03	0.35

Table 2. Key variable comparison between thermodynamic analysis and HYSYS simulation

Units	Variables	Optimisation	Simulation	Relative error (%)
Flash drum	f_{MR}	9020 kg/h		
	f_{HMR}	6625.3 kg/h		
	$F_{CH4\ HMR}$	0.3834	0.3942	2.73
	$F_{C2H6\ HMR}$	0.5746	0.5608	2.47
	$F_{N2\ HMR}$	0.0420	0.0430	2.44
	F_{LMR}	2394.7 kg/h		
	$F_{CH4\ LMR}$	0.6180	0.6170	0.15
	$F_{C2H6\ LMR}$	0.2236	0.2196	1.79
	$F_{N2\ LMR}$	0.1585	0.1634	2.98
	$k1$	1.612	1.565	2.97
	$k2$	0.389	0.392	0.67
	$k3$	3.778	3.650	3.50

Table 3. Compressor operational comparison before and after optimisation.

Compressor	Outlet pressure, bar		Compression ratio		Shaft work, kW	
	Base case	After optimisation	Base Case	After optimisation	Base Case	After Optimisation
C21	2.685	2.723	2.685	2.723	231.53	224.25
C22	7.461	7.666	2.778	2.815	369.34	360.55
C23	18.943	19.765	2.721	2.758	502.59	387.10
C24	52.000	55.000	2.819	2.855	486.10	366.98
Total	–	–	–	–	1589.56	1338.88
				Energy Saving	15.77%	

Table 4. Heat exchanger operational comparison before and after optimisation.

Heat exchanger	Variables	Base case	After optimisation
HX-21	T_{l2} (°C)	-115	-100.0
	T_{v2} (°C)	-115	-135.0
HX-22	T_{n2} (°C)	-130	-128.7
	T_{v3} (°C)	-130	-145
_	f_{MR} (kg/h)	10 980.00	9 020.00
_	f_{HMR} (kg/h)	7 577.40	6 625.30
_	f_{-*MR} (kg/h)	3 402.60	2 394.70

Profound thermodynamic analysis is performed to deliver complete insights of the process. Fig. 3 depicts the temperature-specific enthalpy (T-H) relationship of mixed-refrigerant (MR) streams through the entire process for base and optimised cases for the purpose of comparison. To make phase data clear, the complete phase envelope including the dew point line and the bubble point line of MR is illustrated in figure. In HX21, the outlet hot stream l_2 temperature in the optimised case $(-100℃)$ exceeds that of the base case $(-115℃)$. In contrast, the temperature of another hot stream v_2 $(-135℃)$ is lower than its temperature in the baseline case $(-115℃)$. More importantly, the outlet cold stream m_2 temperature increased from $(-70.6℃)$ in the base case to reach $(-44.72℃)$ in the optimised case. In HX22, the outlet temperature of the cold stream v_5 remained almost the same in both cases at a value of approximately $(-147.6℃)$.

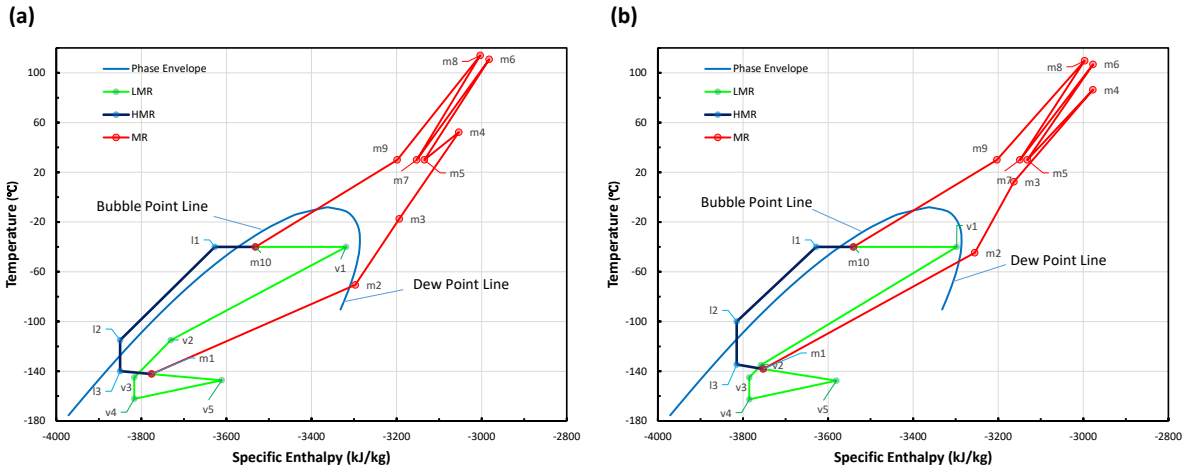

Fig. 3. (T-H) Diagram for MR in (a) Base Case, and (b) Optimized Case

Fig. 4 clearly illustrates the composite curves of HX21 and HX22. On the same graph grid, the corresponding temperature difference of the heat exchange process in baseline case and optimised case is demonstrated. For HX21, maximum temperature difference is about 52.70℃ in the base case, whereas it is reduced to 45.43℃ in the optimised case. This peak on the right side of the curve is a result of the cold stream's transition from the liquid phase into the vapour phase. It is worth noting that at the warm end of HX21, the difference in temperature between the hot and cold composite curves decreased dramatically from 30.06℃ in the base case to settle at a value of 4.72℃ in the optimised case. This means less reversibility of LNG liquefaction process. Similarly, the difference in temperature between the hot and cold composite curves at the warm end of HX22 decreased from 32.29℃ in the base case to 18.85℃ in the optimised case.

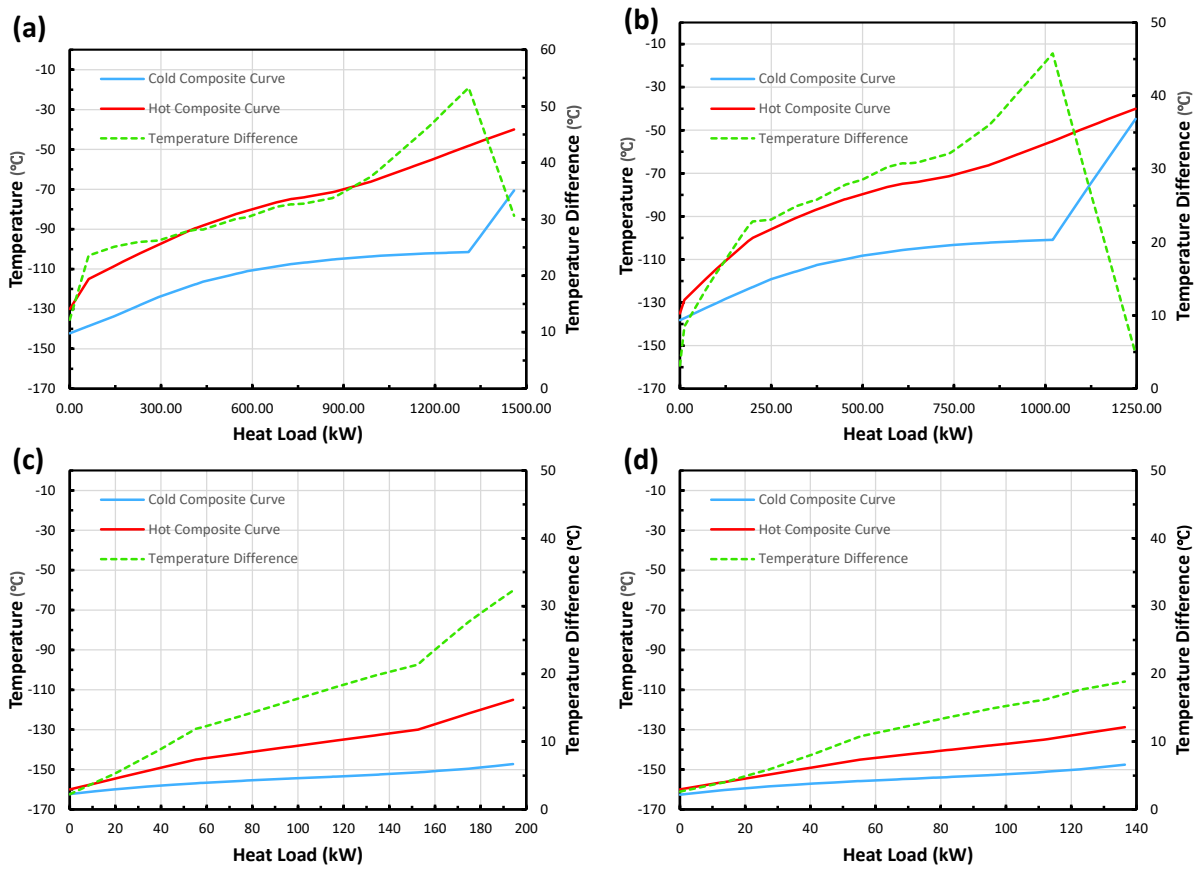

Fig. 4. Composite Curves for LNG Exchangers; (a) HX21 Base Case, (b) HX21 Optimized Case, (c) HX22 Base Case, (d) HX22 Optimized Case

6. Conclusion

The key target of the design and operation of the LNG liquefaction process is to minimise energy consumption. The present work introduces a novel MP technique for optimising LNG synthesis. The optimisation model is developed using thermodynamic analysis, mathematical programming, and meticulous simulation. Excel-based thermodynamic property model scripts were built and validated, then linked with GAMS by GDXXRW Data Exchange facility. LINDO global solver is then employed to solve the model. Eventually, Aspen HYSYS V11 was implemented to test the optimisation outputs to guarantee solution viability. This methodology is accurately applied to a C3MR process synthesis case study where the energy consumption is reduced by 15.77%.

Declaration of competing interest

The authors declare that they have no known competing financial interests or personal relationships that could have appeared to influence the work reported in this paper.

Nomenclature

Sets and indexes

i, j	Indexes of streams
k	Index of a stream status
n	Index of compressor stage
X	Heat exchanger index

Coefficients and parameters

$a_i(T)$	Peng-Robinson attraction parameter for component i at temperature T $\left(cm^6.bar/mol^2\right)$
a_{ij}	Cross PR attraction parameter for components i and j.
$a(T)_m$	Peng-Robinson attraction parameter for the mixture at temperature T $\left(cm^6.bar/mol^2\right)$
b_i	Peng-Robinson attraction parameter for component i $\left(cm^3/mol\right)$
b_m	Peng-Robinson attraction parameter for the mixture $\left(cm^3/mol\right)$
Ω_a, Ω_b	Soave-Redlich-Kwong dimensionless pure component parameters
A_m, B_m	Peng-Robinson Parameters for the mixture at system temperature and pressure
B_i	Peng-Robinson Parameter for the mixture for component i at system temperature and pressure
k_{ij}	Peng-Robinson binary interaction coefficient
m_i, α_i	Peng-Robinson Parameters for component i
T^{max}	Preset upper temperature limit (℃)
ΔT_{min}	Heat exchanger minimum approach temperature difference (℃)
T^{cmax}	Upper limit of the compressor outlet temperature (℃)
$\gamma_i^{(P0)}$	Activity coefficient of liquid condensable component i corrected to zero pressure
γ_i^{∞}	Activity coefficient of non-condensable component i at infinite dilution
φ_i^L	Fugacity coefficient of component i in liquid phase
φ_i^V	Fugacity coefficient of component i in vapour phase
ψ_i	Parameter depending on PR cross-attraction parameter a_{ij} for components i and j

Variables

C_{pi}^{id}	Constant-pressure ideal-gas specific heat capacity $\left(kJ/kmol.K\right)$
Cr_n	Compression ratio of nth stage
$Cr_{uncorrected}$	Uncorrected compression ratio
C_p	Constant-pressure specific heat $\left(kJ/kmol.K\right)$
C_v	Constant-volume specific heat $\left(kJ/kmol.K\right)$
$f_i^{(P0)}$	Fugacity (bar) of pure liquid condensable component i at system temperature T, at standard state, corrected to zero pressure
f_i^{0L}	Fugacity (bar) of pure liquid i at system temperature T at standard state
$H_{h_i^{in}}^X, H_{h_i^{out}}^X$	Mass enthalpy of hot inlet and outlet stream i of heat exchanger X (kJ/kg)
$H_{c_j^{in}}^X, H_{c_j^{out}}^X$	Mass enthalpy of cold inlet and outlet stream j for heat exchanger X (kJ/kg)
$H_{cp_n}^{in}, H_{cp_n}^{out}$	Mass enthalpy of inlet and outlet stream at nth compression stage (kJ/kg)
H_k	Stream mass enthalpy at status k in (kJ/kg)
$\dot{H}_k$	Stream mass enthalpy rate at status k in (kJ/h)
$\Delta H_{h_i}^X$	Mass enthalpy change of hot stream i in heat exchanger X (kJ/kg)
$\Delta H_{c_j}^X$	Mass enthalpy change of cold stream j in heat exchanger X (kJ/kg)
$H^V\ (T,\ P, y_i)$	Enthalpy of a real vapour-phase mixture fluid stream $(kJ/kmol)$
$H_{mix}^{id}(T,\ P, y_i\ )$	Ideal-gas enthalpy of a vapour mixture at pressure P, temperature T, and composition y_i $(kJ/kmol)$
$H_{mix}^R(T,\ P, y_i)$	Residual enthalpy of a vapour mixture at pressure P, temperature T, and composition y_i $(kJ/kmol)$
$H_{i\ (T,P)}^{id}$	Ideal-gas enthalpy of component i $(kJ/kmol)$
$H^L(T,\ x_i)$	Real liquid-phase mixture fluid stream enthalpy $(kJ/kmol)$
$H_i^L(T)$	Real liquid-phase enthalpy of component i in stream $(kJ/kmol)$
$H_i^R\ (T,\ P_i^s)$	Residual enthalpy (kJ/kg) of component i at system temperature T and saturation pressure P_i^s

$\Delta h_{f_i}^0$	Standard heat of formation of component i $(kJ/kmol)$
$H^{id}(T,\ x_i)$	Ideal-gas enthalpy of mixture $(kJ/kmol)$
Δh_{v_i}	Heat of vaporization of component i at system temperature $(kJ/kmol)$
K_i	Vapour- liquid equilibrium ratio (K-factor) of component i
k	Specific heats ratio; isentropic exponent
$\dot{m}_{h_i}.\Delta H_{h_i}^X$	Hot stream i enthalpy rate of change during heat exchange process in heat exchanger X (kJ/h)
$\dot{m}_{c_j}.\Delta H_{c_j}^X$	Cold stream j enthalpy rate of change during heat exchange process in heat exchanger X (kJ/h)
$\dot{m}_k$	Mass flow rate of stream at status k in (kg/h)
n	Polytropic exponent
n_L	Liquid molar fraction of two-phase stream at equilibrium
n_V	Vapour molar fraction of two-phase stream at equilibrium
n_t	Number of moles of two-phase stream
P	System pressure (bar)
P_{ci}	Critical pressure of component i (bar)
$P_{h_i^{in}}, P_{h_i^{out}}$	Hot inlet and outlet stream pressure for a heat exchanger (bar)
$P_{c_j^{in}}, P_{c_j^{out}}$	Cold inlet and outlet stream pressure for a heat exchanger (bar)
$P_{Cp_n}^{in}, P_{Cp_n}^{out}$	Inlet and outlet stream pressure at nth compression stage (bar)
P_k	Pressure of a stream at status k
P_i^s	Saturation pressure of component i at system temperature (bar)
$\dot{Q}_{Hot}^X$	Total hot stream heat load of heat exchanger X (kJ/h)
$\dot{Q}_{Cold}^X$	Total cold stream heat load of heat exchanger X (kJ/h)
R	Universal gas constant $\left(8.314\ {}^{J}/_{mol.K}, 83.14\ {}^{cm^3.bar}/_{mol.K}\right)$
$T_{h_{i,X}}^{in}, T_{h_{i,X}}^{out}$	Hot inlet and outlet stream temperature for heat exchanger X (℃)
$T_{C_{j,X}}^{in} T_{C_{j,X}}^{out}$	Cold inlet and outlet stream temperature for heat exchanger X (℃)
$T_{cp_n}^{in}, T_{cp_n}^{out}$	Inlet or outlet stream temperature at nth compression stage (℃)
T_k	Stream temperature at status k
T	System Temperature (K)
T_{ci}	Critical temperature of component i (K)
T_{pc}	Pseudocritical temperature of the mixture (K)
$\underline{v}$	Molar volume $\left({}^{cm^3}/_{mol}\right)$
ω_i	Acentric factor of component i
$\dot{W}_{cp_n}$	Compressor shaft work at nth compression stage (kW)
$\dot{W}_{total}$	Total shaft work consumption rate (kW)
x^L	Mole fraction of the liquid portion of the system
x^V	Mole fraction of the vapour portion of the system
x_i	Component i Mole fraction in liquid stream
x, y_n	Binary variables
y_i	Component i Mole fraction in vapour stream
Z	Compressibility Factor
z_i	Mole fraction of component i in two-phase stream
Z_i^s	Vapour-phase compressibility factor for component i at P_i^s
Z^V	Vapour-phase compressibility factor
Z^L	Liquid-phase compressibility factor

Functions

f	Vapour Fraction function in Rachford-Rice procedure

Superscripts and subscripts

id	Ideal-gas property
R	Residual property
s	Saturation state
$P0$	Pressure corrected to zero state
∞	Index of infinite dilution state of a noncondensable component
$0L$	Standard state of a pure liquid
max	maximum
m	Mixture property
L	Liquid property
V	Vapour Property

References

[1] "Liquefied natural gas-U.S. Energy Information Administration (EIA)." (accessed Apr. 04, 2023). https://www.eia.gov/energyexplained/natural-gas/liquefied-natural-gas.php

[2] "World LNG Report 2022," IGU. (accessed Apr. 04, 2023). https://www.igu.org/resources/world-lng-report-2022/

[3] Primabudi E, Morosuk T, and Tsatsaronis G. Multi-objective optimisation of propane pre-cooled mixed refrigerant (C3MR) LNG process. Energy, 2019; 185: 492–504. https://doi.org/10.1016/j.energy.2019.07.035

[4] Vaidyaraman S, and Maranas CD. Synthesis of Mixed Refrigerant Cascade Cycles. Chem. Eng. Commun., 2002; 189(8): 1057–1078.https://doi.org/10.1080/00986440213475

[5] Jensen JB, and Skogestad S. Optimal operation of simple refrigeration cycles. Comput. Chem. Eng., 2007; 31(5–6): 712–721.https://doi.org/10.1016/j.compchemeng.2006.12.003

[6] Jensen JB, and Skogestad S. Optimal operation of simple refrigeration cycles. Comput. Chem. Eng., 2007; 31(12): 1590–1601.https://doi.org/10.1016/j.compchemeng.2007.01.008

[7] Aspelund A, Gundersen T, Myklebust J, Nowak MP, and Tomasgard A. An optimisation-simulation model for a simple LNG process. Comput. Chem. Eng.,2010; 34(10): 1606–1617. https://doi.org/10.1016/j.compchemeng.2009.10.018

[8] Alabdulkarem A, Mortazavi A, Hwang Y, Radermacher R, and Rogers P. Optimisation of propane pre-cooled mixed refrigerant LNG plant. Appl. Therm. Eng., 2011; 31(6–7): 1091–1098. https://doi.org/10.1016/j.applthermaleng.2010.12.003

[9] Mortazavi A, Somers C, Alabdulkarem A, Hwang Y, and Radermacher R. Enhancement of APCI cycle efficiency with absorption chillers. Energy, 2010; 35(9): 3877–3882. https://doi.org/10.1016/j.energy.2010.05.043

[10] Mokarizadeh Haghighi Shirazi M, and Mowla D. Energy optimisation for liquefaction process of natural gas in peak shaving plant. Energy, 2010; 35(7): 2878–2885. https://doi.org/10.1016/j.energy.2010.03.018

[11] Khan MS, Karimi IA, Bahadori A, and Lee M. Sequential coordinate random search for optimal operation of LNG (liquefied natural gas) plant. Energy, 2015; 89: 757–767. https://doi.org/10.1016/j.energy.2015.06.021

[12] Ghorbani B, Hamedi M-H, Shirmohammadi R, Hamedi M, and Mehrpooya M. Exergoeconomic analysis and multi-objective Pareto optimisation of the C3MR liquefaction process. Sustain. Energy Technol. Assess., 2016; 17: 56–67. https://doi.org/10.1016/j.seta.2016.09.001

[13] Wang M, Zhang J, Xu Q, and Li K. Thermodynamic-Analysis-Based Energy Consumption Minimization for Natural Gas Liquefaction. Ind. Eng. Chem. Res., 2011; 50(22): 12630–12640. https://doi.org/10.1021/ie2006388

[14] Wang M, Zhang J, Xu Q. Optimal design and operation of a C3MR refrigeration system for natural gas liquefaction. Comput. Chem. Eng., 2012; 39: 84–95. https://doi.org/10.1016/j.compchemeng.2011.12.003

[15] Edgar TF, Himmelblau DM., and Lasdon LS. Optimisation of Chemical Processes, 2nd ed. in McGraw-Hill chemical engineering series. New York: McGraw-Hill, 2001.

[16] Floudas CA. Deterministic Global Optimisation: Theory, Methods And Applications, vol. 37. Springer Science & Business Media, 2013.

[17] Peng D-Y, and Robinson DB. A New Two-Constant Equation of State. Ind. Eng. Chem. Fundam., 1976; 15(1):59–64, Feb. 1976. https://doi.org/10.1021/i160057a011
[18] Rosenthal RE. GAMS, A User's Guide. GAMS Development Corporation, Washington, DC, USA, 2007.
[19] de Vincentis J. Physical Property Methods and Models 11.1.
[20] "Chapter 12 Compression equipment (Including Fans)," in Applied Process Design for Chemical & Petrochemical Plants, Elsevier, 2001, pp. 368–580. https://doi.org/10.1016/S1874-8635(01)80005-4
[21] Hasan MMF, Karimi IA, Alfadala HE, and Grootjans H. Operational modeling of multistream heat exchangers with phase changes. AIChE J., 2009; 55(1): 150–171. https://doi.org/10.1002/aic.11682
[22] Schultz JM. The Polytropic Analysis of Centrifugal Compressors. J. Eng. Power, 1962; 84(1): 69–82. https://doi.org/10.1115/1.3673381
[23] Smith JM. Introduction to chemical engineering thermodynamics J. Chem. Educ., 1950; 27(10): 584. https://doi.org/10.1021/ed027p584.3
[24] Gmehling J, Kleiber M, Kolbe B, and Rarey J. Chemical Thermodynamics for Process Simulation, Second, Completely Revised and Enlarged. in Second Edition. Wiley-VCH, 2019.
[25] Poling BE, Prausnitz JM, and O'Connell JP. The properties of gases and liquids, 5th ed. New York: McGraw-Hill, 2001.
[26] Tester JW, and Modell M. Thermodynamics and Its Applications, Subsequent edition. Upper Saddle River, N.J: Pearson College Div, 1997.
[27] Computer Calculations for Multicomponent Vapor-Liquid and Liquid-Liquid Equilibria.
[28] Rachford HH, and Rice JD. Procedure for Use of Electronic Digital Computers in Calculating Flash Vaporization Hydrocarbon Equilibrium. J. Pet. Technol., 1952; 4(10): 19–3. https://doi.org/10.2118/952327-G
[29] Burden RL, Faires JD, and Burden AM. Numerical Analysis. Cengage Learning, 2015.
[30] LINDO Systems, Inc, LINDO API 13.0 User Manual. Chicago, Illinois, USA: LINDO Systems, Inc., 2019.

To whom correspondence should be addressed: Adel Omar, Petroleum Refining and Petrochemical Engineering Department, Faculty of Petroleum and Mining Engineering, Suez University, Suez, Egypt,
E-mail: adelomar93@icloud.com ORCID: 0009-0002-3240-1100